Diabetes/Metabolism Research and Reviews

WILEY

RESEARCH ARTICLE

Proteomic and Metabolomic Interplay in the Regulation of Energy Metabolism During Obesity and Metabolic Syndrome

Carlos Vinicius F. da Silva[1] | Carlos José F. da Silva[2,3] | Thaís R. Cataldi[4] | Carlos A. Labate[4] | Youssef B. Sade[5] | Sandra Mara N. Scapin[5] | Fabiano L. Thompson[1] | Cristiane Thompson[1] | Carina Maciel da Silva-Boghossian[6] | Eidy de Oliveira Santos[2,3]

[1]Institute of Biology, Federal University of Rio de Janeiro (UFRJ), Rio de Janeiro, Rio de Janeiro, Brazil | [2]Faculty of Biological Sciences and Health, Rio de Janeiro State Univesity (UERJ), Rio de Janeiro, Rio de Janeiro, Brazil | [3]Afya-University of Grande Rio (Afya-Unigranrio), Duque de Caxias, Rio de Janeiro, Brazil | [4]Department of Plant Genetics, Luiz de Queiroz College of Agriculture, University of São Paulo—USP, Piracicaba, São Paulo, Brazil | [5]Department of Macromolecules, National Institute of Metrology, Quality and Technology (INMETRO), Duque de Caxias, Rio de Janeiro, Brazil | [6]Department of Dentistry, Federal University of Rio de Janeiro (UFRJ), Rio de Janeiro, Rio de Janeiro, Brazil

Correspondence: Eidy de Oliveira Santos (eidyos@gmail.com)

Received: 30 March 2025 | **Revised:** 17 June 2025 | **Accepted:** 16 August 2025

Funding: This work was supported by the funding agency FAPERJ, which provided financial resources and grants.

Keywords: metabolic syndrome | metabolome | obesity | omics and interatome | proteome

ABSTRACT

Aim: Explore the influence of obesity and Metabolic Syndrome disorders on the plasma proteome and metabolome, through an integrated analysis.

Materials and Methods: We investigated metabolic and proteomic alterations associated with obesity and MetS, through mass spectrometry, using plasma samples from 49 volunteers, categorized according to BMI, and MetS.

Results: We identified 231 proteins and 77 metabolites. A subset, including DMBT1, Vanin-1, PTPRJ, β-hydroxybutyrate, α-tocopherol, and 5-oxoproline, emerged as potential key players associated with obesity and MetS. By integrating proteomic and metabolomic data, we were able to construct an interactive network involved in metabolic dysfunction, revealing associations between these molecules and clinical parameters, such as BMI, HOMA-IR and HOMA-β.

Conclusions: Our data suggested an interplay between anti-inflammatory (DMBT1, 3-hydroxybutyrate, 5-oxoproline) and pro-inflammatory pathways (Vanin-1, α-tocopherol, PTPRJ) during disorders of obesity and MetS, demonstrating the potential of an integrated multi-omics approach for a better understanding of the mechanism behind obesity-associated metabolic diseases.

1 | Introduction

Obesity is a condition characterized by excessive adipose tissue accumulation [1]. This state triggers a cascade of metabolic dysregulations, potentially leading to the development or worsening of various chronic diseases. The multifaceted impact of obesity on human health includes increased production of inflammatory proteins, fostering chronic systemic inflammation, and significantly contributing to the emergence of obesity-related comorbidities such as metabolic syndrome (MetS) [2, 3].

Previously viewed as a concern primarily for developed nations, the global burden of obesity has significantly increased

in developing countries as well. In 2022, an estimated 2.5 billion adults (≥ 18 years) were overweight, with 890 million of those classified as obese [1]. Reflecting this global trend, data from Brazil's 2023 Telephone Surveillance of Risk and Protective Factors for Chronic Diseases (VIGITEL) [4] revealed that 61.4% and 24.3% of adults were overweight and 24.3% obese. These figures highlight the substantial burden obesity places on healthcare systems worldwide, particularly when considering its association with metabolic diseases such as MetS.

Metabolic syndrome includes some metabolic disorders that significantly elevate susceptibility to developing cardiovascular diseases and type 2 diabetes mellitus (T2DM). The five diagnostic criteria for MetS include hypertriglyceridemia, low HDL cholesterol, increased waist circumference (abdominal obesity), hypertension, and hyperglycemia, with the possibility of including insulin resistance or T2DM itself [5, 6]. Using the NCEP ATP III criteria [7], global prevalence estimates for MetS reached 12.5% in 2021 [8]. In Brazil, a study by De Siqueira Valadares et al. (2022) [9] reported a concerning prevalence of 31% for metabolic syndrome over the past decade (2011–2021) based on the NCEP ATP III criteria.

Emerging evidence suggests that obesity and MetS are associated with significant alterations in both the metabolome and proteome [10, 11]. Studies have identified changes in branched-chain amino acids (BCAAs), such as leucine, isoleucine, and valine, in individuals with obesity. Additionally, alterations in propionylcarnitine, phenylalanine, and docosapentaenoic acid have been observed in individuals with MetS. Proteomic analysis has revealed dysregulation of proteins such as the lysosomal cobalamin transporter ABCD4, vitronectin, and profilin-1 under both conditions [10, 11].

The global surge in obesity and MetS poses a significant health burden [12–14]. Since obesity and MetS are multifactorial, developing novel diagnostic methods to identify individuals at risk is crucial for early intervention and improved clinical outcomes. In this sense, a comprehensive understanding of the molecular alterations in individuals associated with obesity and MetS symptoms is essential to determine underlying mechanisms for diagnoses. Integrating multiomics data offers a powerful approach to elucidate the complex patterns related to clinical response to these conditions and to develop more accurate diagnostic tools and personalized treatment strategies, ultimately improving patient quality of life.

Therefore, we propose here an integrative study of proteomic and metabolomic profiles related to increasing BMI and the MetS disease. Plasma samples from 49 adults from Rio de Janeiro, Brazil, categorized into four nutritional states: normal weight (NW), overweight (OW), obese (OB), and MetS, were analysed. By integrating metabolomics and proteomics data with clinical parameters, we identified significant changes in metabolites and proteins. Our findings revealed alterations in amino acid metabolism, glucose homoeostasis, transport of fatty acids, and inflammatory markers in individuals with obesity and MetS.

2 | Materials and Methods

2.1 | Experimental Design

This study recruited 49 adult volunteers (≥ 18 years old) residing in Rio de Janeiro State, Brazil. This research was approved by the Ethics Committee in Human Research at Unigranrio, RJ, Brazil (approval number: 3,402,791) and was conducted following the ethical principles outlined in the Declaration of Helsinki (1964) and its subsequent amendments. Following a 12-h overnight fast, morning blood collection was performed in a clinical laboratory at the Afya-Unigranrio University, Duque de Caxias, RJ [15]. Participants were categorized according to their Body Mass Index (BMI) as follows: Normal Weight (NW; $n = 13$): BMI between 18.5 kg/m^2 and 24.9 kg/m^2; Overweight (OW; $n = 12$): BMI between 25 kg/m^2 and 29.9 kg/m^2; Obese (OB; $n = 12$): BMI ≥ 30 kg/m^2. MetS was determined according to the NCEP/ATPIII protocol. Volunteers must have at least 3 criteria established by the protocol to be characterized as with MetS. Individuals with abdominal obesity who had only one additional criterion for MetS classification were classified as having obesity only. After homoeostasis model assessment of insulin resistance (HOMA-IR) and β-cell function (HOMA-β) account, twelve (12) individuals were diagnosed with Metabolic Syndrome (MetS; 9 obeses and 3 with OW), following [16, 17].

2.2 | Clinical Evaluation

Clinical examinations were performed following established protocols [18]. The survey included BMI, height, weight, waist circumference, hip circumference, and waist-hip ratio, blood pressure evaluation using the oscillometric method (OMRON 7320) and biochemical blood analysis. Measurements with discrepancies exceeding 10 mmHg for systolic pressure or 5 mmHg for diastolic pressure were discarded to minimize errors [19]. Additionally, HOMA-IR) and HOMA-β) were calculated using previously described formulae [16, 17].

2.3 | Sample Processing

Plasma samples were obtained following established protocols [18]. Briefly, 5 mL of whole blood was collected intravenously after a 12-h fast in EDTA-containing tubes (Vacuplast EDTA K3) to prevent coagulation and stored at −80°C. For protein purification, 50 μL aliquots of plasma were depleted of albumin and immunoglobulins using ProteoPrep Blue Albumin & IgG Depletion columns (Sigma-Aldrich) and eluted proteins were concentrated with Amicon Ultra-0.5 mL 3KD filter devices (Millipore Corporation). Total protein concentration was determined using the Bradford method.

2.4 | Protein Processing for Mass Spectrometry

For mass spectrometry, 10 μg of protein was subjected to an in-solution digestion protocol [20]. The protein was denatured with 0.2% RapiGest Waters, USA) at 80°C for 15 min, followed by reduction with 100 mM DTT at 60°C for 30 min and alkylation

with 300 mM iodoacetamide at room temperature for 30 min. Trypsin digestion was then performed overnight at 37°C with a 1:100 (w/w) enzyme-to-protein ratio using sequencing grade modified trypsin (Promega). The reaction was quenched with 5% (v/v) trifluoroacetic acid (TFA) at 37°C for 90 min to hydrolyse RapiGest. Finally, the peptides were desalted using ZipTip C18 columns (Millipore Corporation) and resuspended in 0.1% TFA solution in (50%) acetonitrile (ACN) 70 μL, that was lyophilizated.

2.5 | Analysis of Plasma Proteins by Mass Spectrometry

Mass spectrometry (MS) analysis was performed using a nanoElute nanoflow chromatography system from Bruker Daltonics (Bremen, Germany) coupled online to a hybrid trapped ion mobility spectrometry-quadrupole time-of-flight mass spectrometer (timsTOF Pro) from Bruker Daltonics. An sample aliquot (1 μL), equivalent to 200 ng of digested peptides, was injected onto an Aurora 2 C18 trap column (1.6 μm, 250 mm × 75 μm) from ionOpticks (Australia). A typical RP gradient (Solvent A: 0.1% FA, 99.9% H2O MilliQ; Solvent B: 0.1% FA, 99.9% CH3CN) was established on a nanoflow liquid chromatography system and separated at a flow rate of 400 nL. min-1. The column temperature was maintained at 50°C. The chromatographic run was 120 min (2%–15% Solvent B for 60 min; increased to 25% at 90 min; increased to 37% at 100 min; increased to 95% at 110 min and finally 95% for 10 min for column washing). The column was coupled online to a timsTOF-Pro with a CaptiveSpray ion source, both from Bruker Daltonik GmbH. The ion transfer capillary temperature was set to 180°C. Ion accumulation for 123 ms and mobility separation were achieved using an input potential ramp from −160V to −20V within 123s.During acquisition, to enable the PASEF method (i.e., ion accumulation parallel to fragmentation), precursor m/z and mobility information were first derived from a Tims-MS full scan experiment with an m/z range of 100–1700. Monocharged precursors were excluded based on their position in the m/z-ion mobility plane, and precursors that reached the target value of 20,000 a.u. were dynamically excluded for 0.4 min. The operational modes of TIMS-ToF, MS, and PASEF were controlled and synchronized using Bruker Daltonik's OtofControl 5.1 instrument control software.

MS raw data were processed using MaxQuant software version 2.4.0.0, specifically designed for mass spectrometry-based protein analysis [21]. The Andromeda search engine integrated into MaxQuant was employed [22]. The default configuration for data acquired on the TimsTof Pro mass spectrometers was utilized. The fragment ion mass tolerance was set to 0.5 Da. Enzyme specificity was trypsin with a tolerance for peptides with up to two undigested cleavage sites. Methionine oxidation (15.994,915 Da) and N-terminal protein acetylation (42.010565 Da) were defined as variable modifications, while cysteine carbamidomethylation (57.021464 Da) was defined as a fixed modification. The minimum peptide length was 7 amino acids. The peptide and protein false discovery rates (FDRs) were set to 1%. Additionally, at least one unique peptide was required for protein identification. Following this data processing step, relative abundance values for all identified proteins were obtained. The database used was the UniProt reviewed *Homo sapiens* database. The download date was 09/11/2023 with a total of 20,436 proteins available (https://www.uniprot.org/uniprotkb?query=human+AND+%28taxonomy_id%3A9606%29&facets=reviewed%3Atrue).

Perseus software version 2.0.9.0 [23] was employed for filtering the proteomics results. Proteins identified only by a modification site, as well as those identified by the reverse database and potential contaminants, were excluded from further analyses. Subsequently, an R programming language script (https://www.R-project.org/) was used to refine the filter based on the percentage of protein presence in the groups and normalize the data by the total ion count (TIC).

2.6 | Extraction of Plasma Metabolites

Metabolites were extracted using 400 μL of ice-cold extraction mixture (acetonitrile:methanol, 1:1, v:v) in a 1:2 sample:extract solution ratio (200 μL). After agitation for 5 min, the samples were centrifuged (Eppendorf, Germany) at 15,000 × g for 10 min at 4°C for deproteinization. The supernatant fractions were then collected and evaporated to dryness using a vacuum concentrator (Concentrator plus, Eppendorf). The resulting dry residues were resuspended in 200 μL of methanol:water (4:1), vortexed, and centrifuged again at 15,000 × g for 10 min at 4°C, and again the supernatant fractions were collected and evaporated to dryness.

2.7 | Mass Spectrometry Analysis of Plasma Metabolites

For GC-MS analysis, a 100 μL aliquot of the metabolite sample was transferred to glass vials (1.5 mL) and lyophilized. In the following step, the sample was derivatized. For derivatization, 30 μL of methoxyamine (15 mg mL-1) in pyridine was added, agitated for 1 min, and then left to stand for 16 h at room temperature in the dark. Silylation was performed by adding 30 μL of MSTFA (N-methyl-trimethylsilyl-trifluoroacetamide) with 1% TMCS (trimethylchlorosilane). The samples were left to stand for 1 h in the dark. Subsequently, 30 μL of Heptane was added. At this stage, a series of alkanes (C12–C40) was used, which allowed the calculation of retention time.

The derivatized samples were automatically injected (1 μL) in splitless mode into a gas chromatograph (8890 GC Agilent Technologie), equipped with a 20 m long × 0.18 mm internal diameter × 0.18 μm film fused silica column (Agilent J&W Scientific). The injection temperature was 280°C, with a flow rate of 20 mL min-1, initiated after 300 s of data acquisition, with the initial temperature of the first column being 80°C, held for 2 min and increased 15°C/minutes until reaching 305°C, then this temperature was held for 2 min. The column effluent was introduced into the ion source of the GC-TOFMS equipment (Pegasus BT, Leco, St. Joseph). The ion source temperature was 250°C, electron beam 70-eV, ionization current of

2.0 mA and 20 spectra s-1 were recorded in the range of 45–800 m/z, and the detector voltage was 1500 V.

The GC-MS data were processed using the ChromaTOF for BT software, version 1.2.0.6, in which baseline correction, deconvolution, retention index (RI) acquisition, retention time (RT) correction, peak identification and alignment were performed, and metabolite identification was performed with the aid of the NIST library, version 2.4 (year 2020). Only metabolites with three or more characteristic masses and a score equal to or greater than 800 were considered valid.

2.8 | Statistical Analysis

The Kolmogorov-Smirnov normality test assessed data distribution, with significant differences investigated using *t*-tests or chi-squared tests. The statistical analyses of the proteomic and metabolomics data were performed in the online MetaboAnalyst 6.0 program (http://www.metaboanalyst.ca/MetaboAnalyst/). Proteins and metabolites were filtered to remain in the abundance matrix only if they had values greater than zero in at least 50% of the samples in at least one of the groups. Quantitative analysis was performed one-way ANOVA with MetaboAnalyst 6.0 to identify statistically significant differences ($p < 0.05$) in normalized abundance between groups. MetaboAnalyst 6.0 was also utilized for Partial Least Squares-Discriminant Analysis (PLS-DA) and Pattern Hunter (PH) analyses to identify group differences. Pearson's correlation analysis performed through PH categorized associations as moderately correlated (0.5–0.7), highly correlated (0.7–0.9), or very highly correlated (0.9–1.0) [24]. The corrplot package (version 0.92) [25] facilitates correlation analysis between proteins and clinical data.

Metabolite set enrichment analysis was performed using MetaboAnalyst 6.0 [26, 27], while protein enrichment analysis was conducted with ShinyGo 0.81 [28, 29]. Both analyses were based on differentially expressed metabolites and proteins.

To identify key features differentiating groups, two multivariate classification algorithms were employed: PLS-DA with VIP (variable importance in the projection) score and Random Forest [30]. Random Forest predicts disease risk based on patient characteristics and identifies the most relevant features (proteins and metabolites in this case) for sample classification [31–33]. In PLS-DA, VIP scores ≥ 1 indicate important variables [34]. To run the performance model, we use the mixOmics package version 6.26, resulting in Receiver Operating Characteristic curves (ROC), confusion matrices, and error rates for plasma protein and metabolite analyses to confirm Random Forest results [35]. We evaluate the model's performance via 10-fold cross-validation, repeated 10 times. In each iteration, we fit a block.splsda model using the pre-specified from our final object on cross-validated samples and then measure the prediction accuracy on the held-out samples. Significance Analysis of Microarrays (SAM) was used to assess the robustness of the proteomics and metabolomics data. Cross-validation was used to assess the generalizability of a predictive model.

3 | Results

3.1 | Demographic and Clinical Evaluation

Supporting Information S1: Table S1 summarizes the demographic and clinical data of the study. The Kolmogorov-Smirnov normality test revealed a normal distribution for demographic and clinical characteristics. No significant differences were observed between the groups for sex, age, height, systolic blood pressure, blood glucose, creatine, urea, total cholesterol, LDL and cholesterol. However, parameters associated with MetS diagnosis, including waist and hip circumferences, HOMA-IR index, HDL, triglycerides, and diastolic blood pressure, demonstrated changes consistent with MetS.

3.2 | Plasma Proteomic and Metabolomic Profiles

An untargeted, gel-free approach using quantitative mass spectrometry was employed to analyse proteomes and metabolomes. This method identified 231 plasma polypeptides, with 53 exhibiting significant differences in abundance (Supporting Information S1: Table S2). Additionally, 77 metabolites were identified in plasma samples, of which 39 displayed differential expression across the groups (Supporting Information S1: Table S3). The max fold change of plasma proteins and metabolites are shown in Supporting Information S1: Tables S2 and S3. To verify the statistical error rate in differentially expressed proteins and metabolisms, the False discovery ratio (FDR) was performed (Supporting Information S1: Tables S2 and S3). A list of all identified proteins and metabolites, like adiponectin, C-reactive protein and Galactopyranose, is also presented (Supporting Information S1: Table S4). Following an ANOVA analysis, pairwise comparisons of protein abundance between groups were performed using a post hoc Tukey's HSD test (Supporting Information S1: Table S2 and S3). Major proteins/metabolites and clinical data are listed in the Supporting Information S1: Table S5. In a prior study by Ferreira da Silva et al. 2024 [10], plasma samples were collected from volunteers in a survey. Plasma samples were prepared for analysis by pooling and subsequently dividing the initial four groups (NW, OW, OB and MetS) into three subgroups. To ensure the robustness and reliability of the results, volunteers were randomly allocated to these subgroups, thereby minimizing potential biases in the analysis. The analysis identified 34 proteins that were common to both the previous study and the current one. This finding highlights that despite the use of different analytical techniques and equipment, which can yield varying results, there are still similarities in the data generated.

All proteomic and metabolomic data underwent verification to assess proteins and metabolites with the highest discriminatory power between groups. RF and VIP scores were employed to select the top 15 most distinctive proteins and metabolites. To validate the reliability of the RF results, ROC (Supporting Information S1: Figures S1 and S2), confusion matrices, and accuracy (Supporting Information S1: Tables S6–S11) were generated for both metabolite and protein features. RF analysis identified 15 key proteins and metabolites as crucial discriminators among the investigated metabolic disorders (Figure 1A,

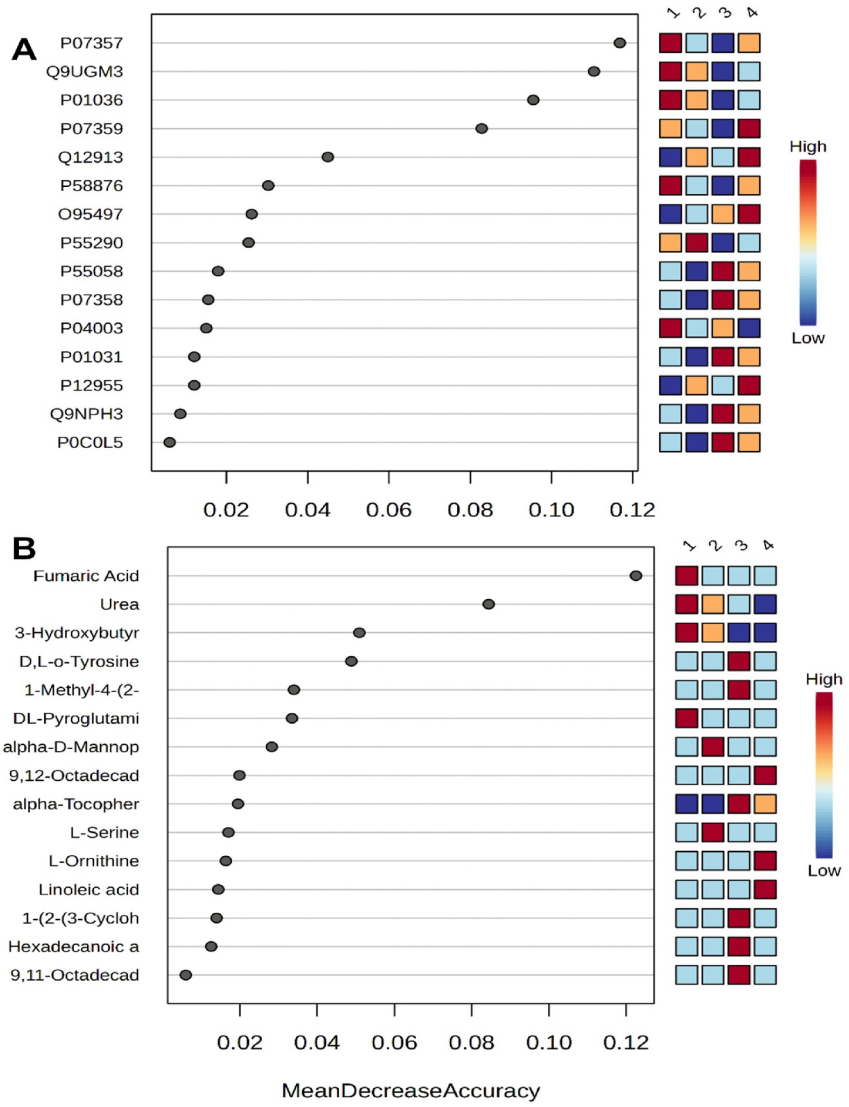

FIGURE 1 | Top 15 key discriminatory proteins and metabolites in RF. Heatmaps displayed alongside the RF model visually depict the relative expression levels of each feature across the study groups. Panel (A) shows the Mean Decrease in Accuracy (MDA) plot for plasma proteins and panel (B) presents the MDA plot for metabolites. P07357 (Complement component C8 alpha chain), Q9UGM3 (DMBT1), P01036 (Cystatin-S), P07359 (Platelet glycoprotein Ib alpha chain), Q12913 (Receptor-type tyrosine-protein phosphatase eta), P58876 (Histone H2B type 1-D), O95497 (Pantetheinase), P55290 (Cadherin-13), P55058 (Phospholipid transfer protein), P07358 (Complement component C8 beta chain), P04003 (C4b-binding protein alpha chain), P01031 (Complement C5), P12955 (Xaa-Pro dipeptidase), Q9NPH3 (Interleukin-1 receptor accessory protein) and P0C0L5 (Complement C4-B). NW (Group 1), OW (Group 2), OB (Group 3), and MetS (Group 4).

B). The five most influential features among plasma proteins were: complement component C8 alpha chain, deleted in malignant brain tumours protein 1, cystatin-S, platelet glycoprotein Ib alpha chain, and receptor tyrosine-protein phosphatase eta. Among plasma metabolites (Figure 2), the five most relevant features identified were: fumaric acid, urea, 3-hydroxybutyric acid, D,L-o-tyrosine, and 1-methyl-4-(2-((trimethylsilyl)oxy) ethyl)piperazine.

In the proteomic analysis, proteins DMBT1, Vanin, and PTRJ were identified based on their unique and total peptides. Specifically, DMBT1 presented 3 unique peptides, Vanin exhibited 7 unique peptides, and PTPRJ was characterized by 5 unique and total peptides. These numbers reinforce the reliability of their identification and quantification in the study.

Significance analysis of proteome and metabolome microarrays identified a set of differentially expressed proteins and metabolites with high statistical confidence. The d values indicate strong differential effects between the analysed groups. The crude and adjusted p values (FDR) reflect a high statistical robustness and a low risk of false positives. This suggests that the findings are biologically relevant and statistically reliable (Supporting Information S1: Table S12).

Cross-validation indicates that the model has good generalization power for metabolite and protein data. With two components, a clear improvement is observed in the accuracy metrics, R^2 and Q^2, suggesting that the model is able to capture significant variation in the data and predict with good reliability. In particular, the high Q^2 values (0.77 for metabolites and 0.81 for

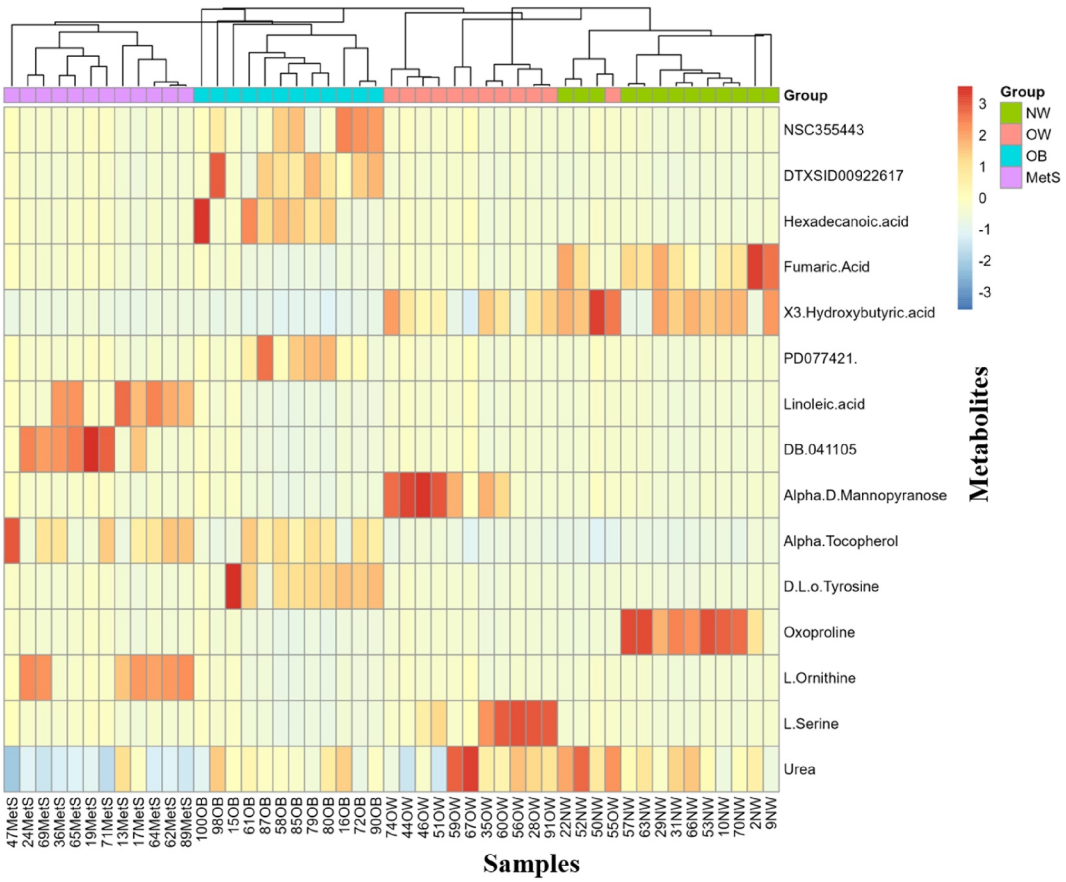

FIGURE 2 | Heatmap of the 15 most relevant plasma metabolites for increased BMI and metabolic syndrome classification using Random Forest.

proteins) suggest good predictive power, with reduced risk of overfitting (Supporting Information S1: Table S13).

Multivariate analysis by PERMANOVA of the plasma proteome and metabolome data demonstrated strong statistical power and robust discrimination among the experimental groups. In the proteomic dataset, a highly significant separation was observed ($F = 58.548$, $R^2 = 0.79605$, $p = 0.001$ based on 999 permutations), indicating that approximately 80% of the data variance is attributable to group classification. Pairwise comparisons (Supporting Information S1: Table S14) confirmed this pattern, with all contrasts showing adjusted p-values < 0.01 and high coefficients of determination (R^2 ranging from 0.45 to 0.83), reflecting clear distinctions between protein profiles. Complementarily, the metabolomic data also showed statistically significant separation among groups ($F = 21.787$; $R^2 = 0.59224$; $p = 0.001$), with around 59% of the total variability explained by group structure. Pairwise PERMANOVA (Supporting Information S1: Table S14) supported this multivariate structure, with R^2 values ranging from 0.46 to 0.62 and adjusted p-values < 0.01 (except for the comparison between groups 1 and 2), reinforcing the consistency of the findings. Together, these results confirm the statistical robustness of the applied omics approaches and support the existence of biologically meaningful differences in the molecular profiles evaluated.

PLS-DA and heatmap of proteomic and metabolomic data revealed distinct clustering patterns among the study groups. Proteomic analysis demonstrated proximity between the NW and OW groups, with OW occupying an intermediate position between NW and OB, as evidenced by overlapping clusters. Conversely, the OB and MetS groups exhibited considerable overlap, indicating proteomic similarity (Supporting Information S1: Figure S3A). Metabolomic data show an overlap between NW and OB groups. Nevertheless, the OB group remained closer to the MetS group in the metabolomic landscape (Supporting Information S1: Figure S3B).

Heatmap analysis revealed distinct patterns of individual changes in the top 15 metabolites (Figure 2) and proteins (Figure 3) from each study group. Notably, both the plasma proteome and metabolome displayed a closer association between the NW and OW groups compared to the obese (OB) group. Interestingly, the OB group exhibited similarity with the MetS group.

Proteomic and metabolomic analyses revealed significant correlations between specific proteins, metabolites and clinical parameters. Using corplot, we observed strong positive correlations between waist circumference and receptor-type tyrosine-protein phosphatase eta and Pantetheinase, while it exhibited strong negative correlations with DMBT1 and Cystatin-S (Supporting Information S1: Figure S4). Similarly, triglycerides showed strong negative correlations with Complement C4-B, Complement C5, phospholipid transfer protein, 1-Methyl-4-(2-((trimethylsilyl)oxy)ethyl)piperazine, and D,L-o-Tyrosine (Supporting Information S1: Figure S5). Further details on moderate correlations can be found in Supporting Information S1: Tables

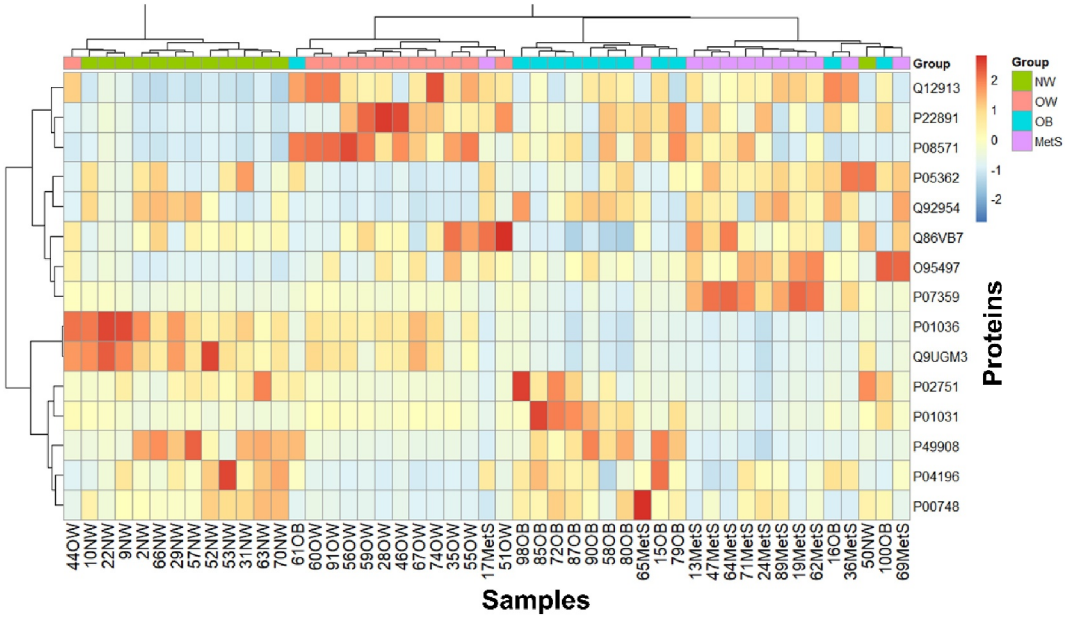

FIGURE 3 | Heatmap of the 15 most relevant plasma proteins. Heatmap analysis revealed the changes detected in the top 15 plasma proteins.

S15 and S16. Pattern Hunter analysis revealed a strong negative correlation between DMBT1 and Cystatin-S proteins and both increased BMI and presence of MetS (Supporting Information S1: Table S17 and Figure 6A). Additionally, moderate negative correlations were observed between the metabolites 3-Hydroxybutyric acid and DL-Pyroglutamic acid and both increased BMI and presence of MetS (Supporting Information S1: Figure S6B and Table S17).

Enrichment analysis revealed that the identified metabolites were associated with SLC-mediated transmembrane transport, disorders of transmembrane transporters, amino acid metabolism, glucose homoeostasis, and fatty acid transport (Supporting Information S1: Figure S7 and Table S18). Similarly, the identified proteins were enriched in biological processes related to immunoglobulin-mediated immune response, complement activation, B cell-mediated immunity, humoural immune response, inflammatory response, and stress response (Supporting Information S1: Figure S8 and Table S19).

3.3 | Segmentation Strategies for Multivariate Analysis

The comparison of the three PLS-DA models of plasma proteome (Supporting Information S1: Figure S9 and S10) highlights both fundamental similarities and differences in how the omics profiles are organized across the distinct groupings: when analysing 'Case × Control' (MetS vs. non-MetS), a nearly binary split is observed, with Component 1 explaining 15.1% of the variance and cleanly separating all individuals with Metabolic Syndrome from the pooled NW + OW + OB group, indicating that the MetS state imposes a dominant multivariate signature that outweighs the subtle BMI variations. In the 'BMI-Only' model (NW vs. OW vs. OB), each component captures only ~9% of the variance, yet a clear incremental gradient of displacement is revealed: NW, OW, and OB form three distinct clusters—albeit partially overlapping at adjacent boundaries—demonstrating that BMI categories, even when isolated from MetS, exhibit differentially marked biochemical profiles; this evidence suggests, moreover, that maintaining these three groups separately is analytically more appropriate than collapsing them into a single 'non-MetS' category. Finally, when all four classes are included simultaneously, Component 1 comes to explain 45.5% of the total variance because it captures both the NW→OW→OB continuum and the additional jump to MetS: NW occupies the far left, OW and OB occupy intermediate positions in a staircase fashion, and MetS forms a separate cluster clearly shifted to the upper right. In summary, these three strategies allow isolation of the pure MetS effect (via Case × Control) and the pure BMI effect (via BMI-Only), and, at the same time, demonstrate how these two effects overlap when considered jointly (via four groups), confirming that BMI progression is gradual and distinct while the transition to MetS represents an abrupt and qualitatively different multivariate shift.

The comparison of the three PLS-DA models (Supporting Information S1: Figure S11 and S12) of plasma metabolites reveals complementary nuances about metabolomic variability as a function of BMI and MetS. In the Case × Control model (NW + OW + OB vs. MetS), Component 1 explains 38.2% of the variance and clearly separates individuals with MetS from the heterogeneous non-MetS pool, but the internal dispersion of this group is amplified by the loss of exclusive metabolites (oxoproline, restricted to NW, and the vitamin, present only in OB and MetS), whose values were zeroed in preprocessing after aggregation, as they did not meet the criterion of presence in at least 50% of the samples, reducing the discriminative resolution within the 'Control.' In contrast, the BMI-Only model (NW vs. OW vs. OB) captures 52.6% in Component 1% and 21.6% in Component 2, revealing three highly cohesive and ordered clusters (NW→OW→OB) with minimal overlap, thanks to the retention of category-specific metabolites and the strong

biochemical progression as BMI increases. Finally, when including all four classes, Component 1 accounts for 64.8% of the total variance by synthesizing both the BMI continuum and the additional 'leap' to MetS: NW, OW, and OB are positioned in a staggered manner on the left, while the MetS cluster shifts abruptly to the upper right corner. Together, these results demonstrate that, although the binary MetS versus non-MetS separation highlights a strong disease effect, the isolated BMI analysis preserves subtle and gradual metabolomic signals that are lost in aggregation, justifying the maintenance of NW, OW, and OB as distinct groups to capture the full spectrum of pre-pathological metabolic changes.

3.4 | Plasma Interactome

R package mixOmics was employed to integrate metabolomic and proteomic data for a comprehensive analysis of Metabolic Syndrome. As shown in Supporting Information S1: Figure S13, the first components of each data set exhibited strong correlations, indicating a close relationship between metabolic and proteomic profiles. Additionally, the colour-coding scheme in the figure highlights the discriminatory power of the first component in separating MetS cases from controls. Clustered Image Map (CIM) analysis, utilizing proteins and metabolites identified as key features in the first principal component, demonstrated effective discrimination among sample groups (Supporting Information S1: Figure S14).

Figure 4A presents a Circos plot of the correlation among selected proteins and metabolites. Positive and negative associations are represented by links connecting the nodes. Fumaric acid exhibited strong positive (Supporting Information S1: Table S20) correlations with Cystatin S and Histone H2B type 1-D, while Complement protein C4-B was strongly correlated with D,L-o-Tyrosine. The predictive performance of models based on plasma proteins and metabolites was evaluated using receiver operating characteristic (ROC) curves (Figure 4B and D). Both models demonstrated excellent discriminative ability, with areas under the curve (AUC) exceeding 0.9. The relevance network (Figure 4C) identified protein-metabolite interactions, with Interleukin-1 receptor accessory protein (Q9NPH3) and Deleted in malignant brain tumours 1 protein (Q9UGM3) showing associations with six metabolites, and Alpha Tocopherol and Fumaric Acid correlating with eight and six proteins, respectively.

4 | Discussion

Obesity and MetS represent significant global health challenges. To elucidate the underlying molecular mechanisms, we

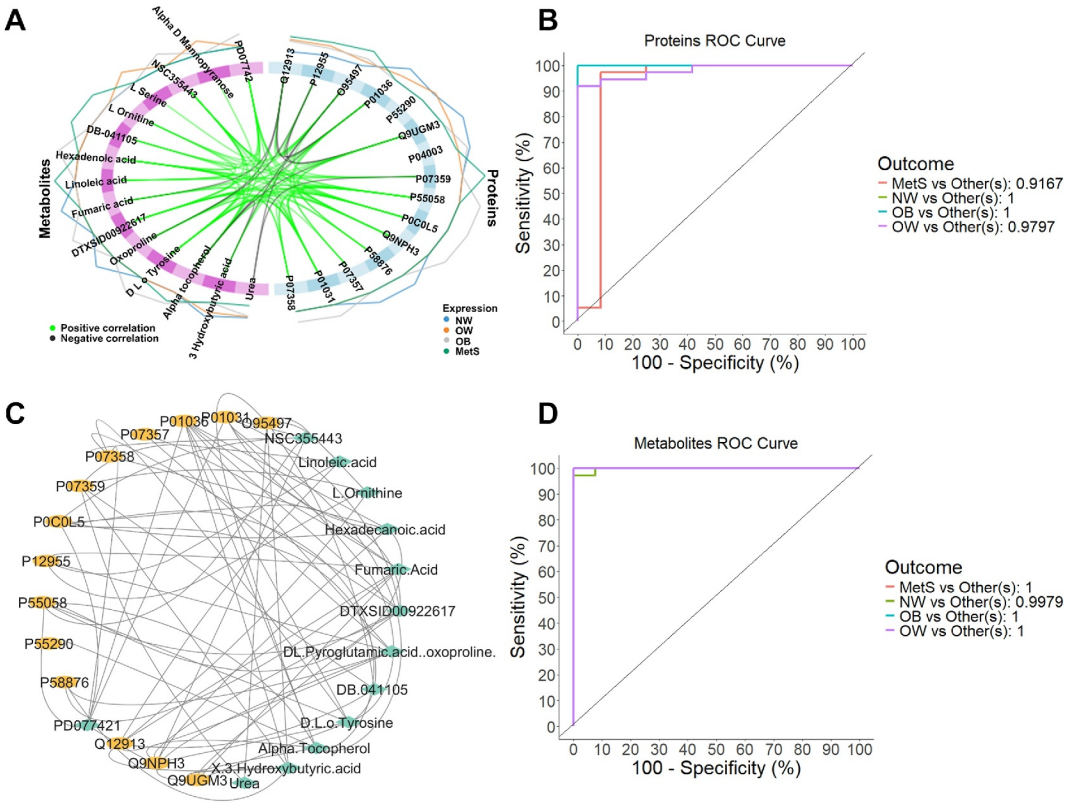

FIGURE 4 | Correlation network among selected features. (A) The diagnostic performance of protein-based and metabolite-based models (B, D) and the protein-metabolite interaction network (C). (A) Presents a circular visualization of features, with links representing positive and negative correlations. (B and D) Display receiver operating characteristic (ROC) curves and corresponding area under the curve (AUC) values for protein and metabolite models, respectively, using one-versus-all comparisons. (C) Illustrates the relevance network, highlighting key protein-metabolite, orange and green, respectively, interactions within the first principal component. Positive and negative associations are represented by links connecting the nodes (A).

conducted a cross-sectional study investigating the metabolic and proteomic profiles of individuals with varying degrees of BMI and MetS. As expected, we observed significant increases in anthropometric and metabolic parameters, including weight, waist circumference, blood pressure, glucose, insulin resistance, and lipid profiles, in individuals with higher BMI and MetS. Through a comprehensive and integrated analysis of protein and metabolite profiles, we identified significant alterations associated with increasing BMI and MetS. These results provide valuable insights into the underlying mechanisms of obesity and MetS, as the dysregulation of key metabolic pathways and immune responses may lead to the identification of novel biomarkers for early diagnosis and targeted therapies.

Deleted in Malignant Brain Tumor 1 (DMBT1), a member of the scavenger receptor cysteine-rich superfamily, is a versatile protein with roles in diverse biological processes. Expressed in epithelial and non-epithelial tissues, DMBT1 plays a crucial role in innate immunity, inflammation, tumour suppression, and epithelial homoeostasis [36]. Previous studies have linked increased DMBT1 expression to improved cancer prognosis, suggesting its potential as a protective factor. Additionally, DMBT1 has been shown to inhibit the production of pro-inflammatory cytokines, including IL-6, TNF-α, IL-8, IL-10, and granulocyte colony-stimulating factor (G-CSF), further supporting its anti-inflammatory properties [37, 38]. Our findings reveal a significant inverse correlation between DMBT1 expression and increasing BMI, with a notable decrease in overweight individuals compared with normal weight controls (Figure 5). In volunteers with obesity and MetS, DMBT1 expression was undetectable. Furthermore, DMBT1 expression was positively correlated with metabolic markers such as fumaric acid, 5-Oxoproline and 3-hydroxybutyrate, while negatively correlated with insulin resistance and anthropometric measures. Given its anti-inflammatory properties, DMBT1 may play a protective role against obesity and MetS, potentially through its anti-inflammatory properties. These findings suggest that DMBT1 expression correlates with key clinical features of obesity and MetS, indicating a potential role for this protein in the pathophysiology of these conditions.

Pantetheinase, also known as vascular non-inflammatory molecule-1 (Vanin-1), is a protein expressed in various tissues, including the kidneys, liver, and intestine. This enzyme catalyses the hydrolysis of pantethine into pantothenic acid (vitamin B5), a precursor for coenzyme A synthesis, suggesting a potential role in lipid metabolism [39, 40]. Beyond its metabolic function, Vanin-1 exhibits pro-inflammatory properties. It antagonizes the anti-inflammatory effects of Peroxisome Proliferator-Activated Receptor Gamma (PPAR-γ), leading to decreased antioxidant enzyme activity and increased oxidative stress [41]. Several studies have linked elevated Vanin-1 levels to metabolic disorders. Positive correlations have been observed between Vanin-1 expression and BMI, waist circumference, and HOMA-IR. Furthermore, increased Vanin-1 levels have been associated with overweight, obesity, T2DM, and pro-inflammatory markers such as inducible nitric oxide synthase (iNOS), tumor necrosis factor-alpha (TNF-α), monocyte chemoattractant protein-1 (MCP-1), and transforming growth factor-beta1 (TGF-β1). It has been suggested that Vanin-1 may contribute to the development and progression of metabolic diseases by promoting inflammation and oxidative stress [42, 43]. Our findings demonstrate a significant positive correlation between Vanin-1 expression and increasing BMI and MetS. Notably, Vanin-1 was not detected in the normal weight group (Figure 5). Furthermore, we observed strong positive correlations between Vanin-1 and various metabolic parameters, including body weight, waist circumference, hip circumference, insulin, HOMA-β, and HOMA-IR. Conversely, a negative correlation was found between Vanin-1 and HDL-C. Interestingly, Vanin-1 exhibited negative correlation with specific metabolites, such as fumaric acid, 3-

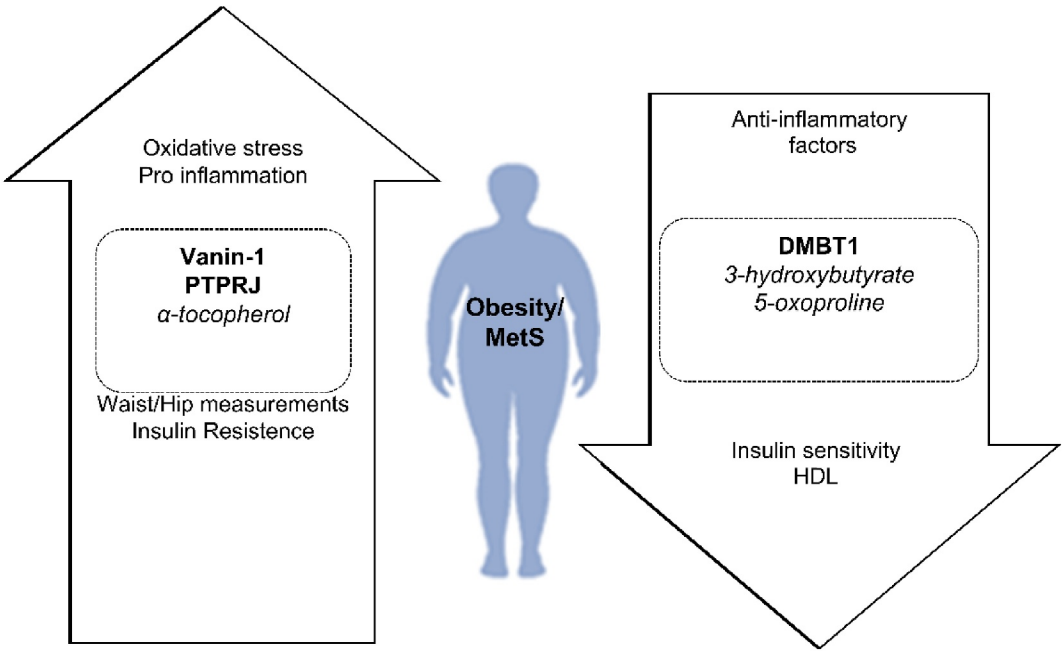

FIGURE 5 | Pro- and anti-inflammatory factors in obesity and metabolic syndrome and their impact on metabolic disorder and inflammation.

hydroxybutyric acid, and D-pyroglutamic acid, while showing a positive correlation with α-tocopherol. Our findings provide further evidence for the role of Vanin-1 in metabolic dysregulation. The significant correlation between Vanin-1 expression and various metabolic parameters in the overall MetS phenotype highlights its potential use for the identification of metabolic syndrome in clinical practice.

Protein-tyrosine phosphatase receptor type J (PTPRJ), also known as density-enhanced phosphatase-1 (DEP-1), is a transmembrane protein with a multifaceted role in regulating a wide array of physiological and pathological processes [44, 45]. PTPRJ has been implicated as a negative regulator of insulin and leptin signalling pathways. PTPRJ knockout mice exhibit enhanced insulin sensitivity and glucose homoeostasis, suggesting a role for PTPRJ in modulating insulin signalling [45, 46]. Moreover, PTPRJ negatively regulates leptin signalling by inhibiting Janus Kinase 2 (JAK2) activation, a critical step in leptin-induced signalling cascades. Reduced PTPRJ expression in mice has been linked to increased leptin sensitivity and decreased body weight gain [47]. Our findings indicate that PTPRJ expression is significantly upregulated in individuals with overweight, obese, and MetS, suggesting a potential role in the pathogenesis of these metabolic disorders (Figure 5). PTPRJ exhibited positive correlations with anthropometric parameters, insulin and HOMA-IR, and negatively correlated with specific metabolites, including DL-Pyroglutamic acid and fumaric acid. Given the role of PTPRJ in regulating insulin and leptin signalling, we suggest that its overexpression may be associated with excessive weight gain and MetS, making this protein a potential target for therapeutic strategies for metabolic disorders.

3-Hydroxybutyrate (β-hydroxybutyrate), a primary ketone body, has garnered significant attention for its potential therapeutic applications. The ketogenic diet, characterized by its high-fat, low-carbohydrate composition, induces ketosis, leading to elevated β-hydroxybutyrate levels. Emerging research suggests that β-hydroxybutyrate possesses potent anti-inflammatory properties, offering a promising avenue for the management of various inflammatory diseases, including cardiovascular disorders [48–50]. In a recent study, severely obese individuals were subjected to an 8-week, low-calorie, milk-based meal replacement program. A significant correlation was observed between weight loss and increased fasting β-hydroxybutyrate levels after two and 8 weeks [51]. Preclinical studies in murine models have demonstrated the glycaemic effect of β-hydroxybutyrate. In Zhang et al. study, β-hydroxybutyrate reduced fasting blood glucose levels, improved glucose tolerance, and enhanced insulin sensitivity [52]. In our cohort, β-hydroxybutyrate was exclusively detected in individuals classified as normal weight or overweight (Figure 5). Notably, negative correlations were found between β-hydroxybutyrate levels and various parameters, including BMI, waist circumference, hip circumference, insulin resistance, and the proteins Vanin-1 and PTPRJ. Conversely, a positive correlation was observed with DMBT1. While previous research has linked β-hydroxybutyrate to insulin resistance and fasting glucose, our findings show its negative association with other clinical parameters and proteins associated with MetS pathology, suggesting its potential as a biomarker for a healthy metabolic state.

Vitamin E, particularly α-tocopherol, possesses potent antioxidant properties and has been implicated in various biological processes, including inflammation and oxidative stress [53, 54]. Some studies have reported a positive correlation between serum α-tocopherol levels and markers of metabolic syndrome, such as hypertriglyceridemia, hyperglycemia, and hypertension. However, the exact mechanisms underlying these associations remain unclear [55, 56]. Elevated α-tocopherol levels have been demonstrated to be associated with an increased risk of developing MetS [57]. Our study demonstrates a strong association between elevated α-tocopherol levels and metabolic dysfunction, particularly in individuals with obesity and MetS (Figure 5). The exclusive detection of α-tocopherol in these individuals, coupled with its positive correlation with insulin resistance and other anthropometric markers (mass, waist and hip circumference), reinforces the role of this vitamin in the pathogenesis of metabolic disorders, indicating a complex interplay between oxidative stress, inflammation, and metabolic health.

5-Oxoproline (5-OP), synonymously referred to as pyroglutamic acid or pidolic acid, is an amino acid that serves as an intermediate in the eukaryotic γ-glutamyl cycle. This molecule undergoes enzymatic conversion to glutamate via 5-oxoprolinase [58]. Multiple studies have consistently reported decreased levels of 5OP in individuals with insulin resistance, demonstrating a negative correlation with the HOMA-IR. Studies have reported an inverse association between pyroglutamic acid levels and the risk of developing type 2 diabetes, hypertension and gestational diabetes. These findings underscore the potential correlation between 5OP and metabolic dysfunction [59–61]. Remarkably, 5OP was exclusively detected in our normal weight cohort (Figure 5). A negative correlation was observed between 5OP levels and key metabolic parameters, including BMI, waist circumference, HOMA-IR, and insulin concentrations. Additionally, 5OP exhibited inverse associations with the proteins Vanin-1 and PTPRJ, while demonstrating a positive correlation with DMBT1. Our findings further support the association between 5OP and insulin resistance, while also suggesting potential links to other metabolic alterations. The exclusive detection of 5-OP in the normal weight cohort, coupled with its inverse correlations with key metabolic parameters such as BMI, HOMA-IR, and insulin, suggests a potential role for 5-OP in maintaining metabolic homoeostasis.

The interaction among the three proteins, DMBT1, Vanin-1, and PTPRJ, and the three metabolites, 3-hydroxybutyrate, α-tocopherol, and 5-oxoproline, reveal a complex network of correlations associated with metabolic and inflammatory regulation in the context of obesity and metabolic syndrome. The expression of DMBT1, with its anti-inflammatory properties, positively correlates with 3-hydroxybutyrate and 5-oxoproline, suggesting a protective role against metabolic dysfunctions, while showing a negative correlation with insulin resistance parameters and OW and obese features. In contrast, Vanin-1, with pro-inflammatory characteristics, and PTPRJ, the negative regulator of insulin and leptin signalling

pathways, present positive correlations with obesity and insulin resistance markers, along with a negative correlation with 3-hydroxybutyrate and 5-oxoproline, reinforcing its role in metabolic dysfunction. The metabolite α-tocopherol, positively correlated with Vanin-1, appears to reflect a pro-inflammatory environment linked to individuals with obesity and MetS. Thus, the balance among these components suggests a critical interplay between anti-inflammatory (DMBT1, 3-hydroxybutyrate, 5-oxoproline) and pro-inflammatory pathways (Vanin-1, α-tocopherol, PTPRJ) in the regulation of energy metabolism and the development of metabolic disorders.

Our findings demonstrate significant metabolic and proteomic alterations associated with increasing BMI and the development of MetS. The identification of key patterns, including DMBT1, β-hydroxybutyrate, Vanin-1, and 5-OP, provides novel insights into the underlying mechanisms of these complex disorders. The observed correlations between these proteins, metabolites and clinical parameters, such as insulin, HOMA-IR, HOMA- β and anthropometric parameters, highlight their potential to better understand the mechanisms related to obesity and MetS and the possible use of these molecules in diagnosis. Interactome analysis further elucidated the intricate relationships between proteins and metabolites, revealing potential regulatory networks involved in metabolic dysfunction. These findings underscore the importance of a multi-omics approach in understanding the complex aetiology of obesity and MetS.

Our findings reveal significant metabolic and proteomic alterations associated with increasing BMI and the metabolic syndrome (MetS). The identification of key molecular signatures, including DMBT1, β-hydroxybutyrate, Vanin-1 and 5-OP, offers novel insights into the complex biological mechanisms underlying these disorders. Despite the modest sample size, the study reflects a carefully controlled experimental design, optimized within the operational constraints of the research center, including consecutive weeks of exclusive equipment use. This work is exploratory in nature and aims to advance our understanding of systemic metabolic and proteomic changes in individuals with obesity and MetS. The prioritization of analytical depth in both plasma proteome and metabolome, allowed us to identify biologically relevant candidates for biomarker development. While the GC-MS platform employed here offers robust quantification of key metabolites, its intrinsic limitations, particularly in detecting non-volatile compounds and high-molecular-weight lipids, necessarily constrain the breadth of metabolic coverage. Nonetheless, the strong correlations observed between specific proteins, metabolites (e.g., insulin, HOMA-IR, HOMA-β), and anthropometric parameters reinforce the biological validity of our findings. Moreover, interactive analysis highlighted regulatory networks implicated in metabolic dysfunction, supporting the utility of multi-omics approaches to understand complex disorders associated with obesity and MetS. Taken together, these findings not only provide a foundation for future hypothesis-driven investigations but also underscore the importance of integrating complementary technologies to achieve a more comprehensive view of metabolic disorders. While some methodological limitations are acknowledged, the strength of the observed associations and the coherence of the biological signals identified affirm the significance of the study within its exploratory scop.

Author Contributions

Carlos Vinicius F. da Silva: statistical analysis, analysis and interpretation of data, writing – original draft, visualisation and acquisition of data. **Carlos José F. da Silva:** statistical analysis, analysis and interpretation of data. **Thaís R. Cataldi:** visualisation and acquisition of data, analysis and interpretation of data. **Carlos A. Labate:** visualisation and acquisition of data, analysis and interpretation of data. **Yousse B. Sade:** analysis and interpretation of data. **Sandra Mara N. Scapin:** analysis and interpretation of data. **Fabiano L. Thompson:** critical revision of the manuscript for important intellectual content. **Cristiane Thompson:** critical revision of the manuscript for important intellectual content. **Carina Maciel da Silva-Boghossian:** Critical revision of the manuscript for important intellectual content. **Eidy de Oliveira Santos:** critical revision of the manuscript for important intellectual content.

Acknowledgements

We extend our gratitude to all the volunteers who participated in this study. We also thank the National Institute of Metrology, Quality and Technology (Inmetro) for their support in sample preparation and the laboratory of the Laboratory of Functional Genetics of Plants at USP ESALQ University for the mass spectrometry (MS) analysis. This work was supported by the funding agency FAPERJ, which provided financial resources and grants.

Conflicts of Interest

The authors declare no conflicts of interest.

Data Availability Statement

The mass spectrometry raw data can be accessed in PRIDE with the dataset identifier PXD053774 (https://www.ebi.ac.uk/pride/) and are publicly available as of the date of publication. Any additional information required to reanalyse the data reported in this paper is available from the lead contact upon request.

Peer Review

The peer review history for this article is available at https://www.webofscience.com/api/gateway/wos/peer-review/10.1002/dmrr.70090.

References

1. World Health Organization, Obesity and Overweight, Accessed on, June 6, 2024, https://www.who.int/news-room/fact-sheets/detail/obesity-and-overweight.

2. S. P. Weisberg, D. McCann, M. Desai, M. Rosenbaum, R. L. Leibel, and A. W. Ferrante Jr, "Obesity Is Associated With Macrophage Accumulation in Adipose Tissue," *Journal of Clinical Investigation* 112, no. 12 (2003): 1796–1808, https://doi.org/10.1172/jci200319246.

3. R. Cancello, C. Henegar, N. Viguerie, et al., "Reduction of Macrophage Infiltration and Chemoattractant Gene Expression Changes in White Adipose Tissue of Morbidly Obese Subjects After Surgery-Induced Weight Loss," *Diabetes* 54, no. 8 (2005): 2277–2286, https://doi.org/10.2337/diabetes.54.8.2277.

4. M. da Saúde, *Secretaria de Vigilância em Saúde e Ambiente, Departamento de Análise Epidemiológica e Vigilância de Doenças Não Transmissíveis. Vigitel Brasil 2023: vigilância de fatores de risco e proteção para doenças crônicas por inquérito telefônico: estimativas sobre frequência e distribuição sociodemográfica de fatores de risco e proteção para doenças crônicas nas capitais dos 26 estados brasileiros e no Distrito Federal em 2023 [recurso eletrônico]* (Brasília: Ministério da Saúde, 2023).

5. G. Reaven, "Role of Insulin Resistance in Human Disease," *Diabetes* 37, no. 12 (1988): 1595–1607, https://doi.org/10.2337/diab.37.12.1595.

6. H. Robberecht, T. D. Bruyne, and N. Hermans, "Biomarkers of the Metabolic Syndrome: Influence of Selected Foodstuffs, Containing Bioactive Components," *Phytochemistry Reviews* 17, no. 2 (2018): 351–377, https://doi.org/10.1007/s11101-017-9538-9.

7. Expert Panel on Detection, Evaluation, "Treatment of High Blood Cholesterol in Adults. Executive Summary of the Third Report of the National Cholesterol Education Program (NCEP) Expert Panel on Detection, Evaluation, and Treatment of High Blood Cholesterol in Adults (Adult Treatment Panel III)," *JAMA* 285, no. 19 (2001): 2486–2497, https://doi.org/10.1001/jama.285.19.2486.

8. J. J. Noubiap, J. R. Nansseu, E. Lontchi-Yimagou, et al., "Global, Regional, and Country Estimates of Metabolic Syndrome Burden in Children and Adolescents in 2020: A Systematic Review and Modelling Analysis," *Lancet Child Adolescence Health* 6, no. 3 (2022): 158–170, https://doi.org/10.1016/S2352-4642(21)00374-6.

9. L. T. De Siqueira Valadares, L. S. B. De Souza, V. A. Salgado Júnior, L. de Freitas Bonomo, L. R. de Macedo, and M. Silva, "Prevalence of Metabolic Syndrome in Brazilian Adults in the Last 10 Years: A Systematic Review and Meta-Analysis," *BMC Public Health* 22, no. 1 (2022): 327, https://doi.org/10.1186/s12889-022-12753-5.

10. L. Szczerbinski, G. Wojciechowska, A. Olichwier, et al., "Untargeted Metabolomics Analysis of the Serum Metabolic Signature of Childhood Obesity," *Nutrients* 14, no. 1 (2022): 214, https://doi.org/10.3390/nu14010214.

11. C. V. Ferreira Da Silva, C. J. F. Da Silva, Y. Bacila Sade, et al., "Prospecting Specific Protein Patterns for High Body Mass Index (BMI), Metabolic Syndrome and Type 2 Diabetes in Saliva and Blood Plasma From a Brazilian Population," *Proteomics - Clinical Applications* 18, no. 6 (2024): e202300238, https://doi.org/10.1002/prca.202300238.

12. A. Okunogbe, R. Nugent, G. Spencer, J. Powis, J. Ralston, and J. Wilding, "Economic Impacts of Overweight and Obesity: Current and Future Estimates for 161 Countries," *BMJ Global Health* 7, no. 9 (2022): e009773, https://doi.org/10.1136/bmjgh-2022-009773.

13. H. Zhang, X. D. Zhou, M. D. Shapiro, et al., "Global Burden of Metabolic Diseases," *Metabolism* 160 (2024): 1990–2021, https://doi.org/10.1016/j.metabol.2024.155999.

14. S. J. Ricardo, M. Y. C. Araujo, L. L. D. Santos, et al., "Burden of Metabolic Syndrome on Primary Healthcare Costs Among Older Adults: A Cross-Sectional Study," *Sao Paulo Medical Journal* 142, no. 6 (2024): e2023215, https://doi.org/10.1590/1516-3180.2023.0215.R1.13052024.

15. C. J. F. D. Silva, C. V. F. D. Silva, A. M. Cardoso, and E. de Oliveira Santos, "Exploring Clinical Parameters and Salivary Microbiome Profiles Associated With Metabolic Syndrome in a Population of Rio de Janeiro, Brazil," *Archives of Oral Biology* 175 (July 2025): 106251, https://doi.org/10.1016/j.archoralbio.2025.106251.

16. B. Geloneze, A. C. J. Vasques, C. F. C. Stabe, et al., "HOMA1-IR and HOMA2-IR Indexes in Identifying Insulin Resistance and Metabolic Syndrome: Brazilian Metabolic Syndrome Study (BRAMS)," *Arquivos Brasileiros de Endocrinologia e Metabologia* 53, no. 2 (2009): 281–287, https://doi.org/10.1590/s0004-27302009000200020.

17. R. Gong, Y. Liu, G. Luo, and L. Yang, "Dietary Magnesium Intake Affects the Vitamin D Effects on HOMA-β and Risk of Pancreatic β-cell Dysfunction: A Cross-Sectional Study," *Frontiers in Nutrition* 9 (2022): 84974, https://doi.org/10.3389/fnut.2022.849747.

18. C. V. F. Da Silva, Y. B. Sade, S. M. N. Scapin, P. E. C. Leite, C. M. Da Silva-Boghossian, and E. O. Santos, "Relevance of Obesity and Overweight to Salivary and Plasma Proteomes of Human Young Adults From Brazil," *Brazilian Journal of Development* 8, no. 2 (2022): 13981–14001, https://doi.org/10.34117/bjdv8n2-363.

19. J. Liu, Y. Li, J. Li, D. Zheng, and C. Liu, "Sources of Automatic Office Blood Pressure Measurement Error: A Systematic Review," *Physiological Measurement* 43 (2022): 9, https://doi.org/10.1088/1361-6579/ac890e.

20. L. F. Boaretto, M. T. V. Labate, L. M. Franceschini, et al., "Proteomics Reveals an Increase in the Abundance of Glycolytic and Ethanolic Fermentation Enzymes in Developing Sugarcane Culms During Sucrose Accumulation," *Frontiers of Plant Science* 12 (2021): 716964, https://doi.org/10.3389/fpls.2021.716964.

21. J. Cox and M. Mann, "MaxQuant Enables High Peptide Identification Rates, Individualized p.p.b.-Range Mass Accuracies and Proteome-Wide Protein Quantification," *Nature Biotechnology* 26, no. 12 (2008): 1367–1372, https://doi.org/10.1038/nbt.1511.

22. J. Cox, N. Neuhauser, A. Michalski, R. A. Scheltema, J. V. Olsen, and M. Mann, "Andromeda: A Peptide Search Engine Integrated into the MaxQuant Environment," *Journal of Proteome Research* 10, no. 4 (2011): 1794–1805, https://doi.org/10.1021/pr101065j.

23. S. Tyanova and J. Cox, "Perseus: A Bioinformatics Platform for Integrative Analysis of Proteomics Data in Cancer Research," in *Cancer Systems Biology*, L. Von Stechow, ed, Vol. 1711, (Methods Mol Biol 2018), 133–148, https://doi.org/10.1007/978-1-4939-7493-1_7.

24. D. E. Hinkle, W. Wiersma, and S. G. Jurs, *Applied Statistics for the Behavioral Sciences*, 5th ed. (Houghton Mifflin, 2003), 756.

25. T. Wei and V. Simko, R Package 'corrplot': Visualization of a Correlation Matrix. Version 0.92, https://github.com/taiyun/corrplot2021.

26. Y. Lu, Z. Pang, and J. Xia, "Comprehensive Investigation of Pathway Enrichment Methods for Functional Interpretation of LC-MS Global Metabolomics Data," *Briefings in Bioinformatics* 24, no. 1 (2023): bbac553, https://doi.org/10.1093/bib/bbac553.

27. J. Xu, J. Li, Y. Li, X. Shi, H. Zhu, and L. Chen, "Multidimensional Landscape of SA-AKI Revealed by Integrated Proteomics and Metabolomics Analysis," *Biomolecules* 13, no. 9 (2023): 1329, https://doi.org/10.3390/biom13091329.

28. S. X. Ge, D. Jung, and R. Yao, "ShinyGO: A Graphical Gene-Set Enrichment Tool for Animals and Plants," *Bioinformatics* 36, no. 8 (2020): 2628–2629, https://doi.org/10.1093/bioinformatics/btz931.

29. M. C. Carbajo-García, E. Juarez-Barber, M. Segura-Benítez, et al., "H3k4me3 Mediates Uterine Leiomyoma Pathogenesis via Neuronal Processes, Synapsis Components, Proliferation, and Wnt/β-Catenin and TGF-β Pathways," *Reproductive Biology and Endocrinology* 21, no. 1 (2023): 9, https://doi.org/10.1186/s12958-023-01060-2.

30. A. M. Koenig, A. Karabatsiakis, T. Stoll, et al., "Serum Profile Changes in Postpartum Women With a History of Childhood Maltreatment: A Combined Metabolite and Lipid Fingerprinting Study," *Scientific Reports* 8, no. 1 (2018): 3468, https://doi.org/10.1038/s41598-018-21763-6.

31. L. Breiman, "Random Forests," *Machine Learning* 45, no. 1 (2001): 5–32, https://doi.org/10.1023/a:1010933404324.

32. T. H. Sun, C. C. Wang, Y. L. Wu, K. C. Hsu, and T. H. Lee, "Machine Learning Approaches for Biomarker Discovery to Predict Large-Artery Atherosclerosis," *Scientific Reports* 13, no. 1 (2023): 15139, https://doi.org/10.1038/s41598-023-42338-0.

33. E. Alladio, F. Trapani, L. Castellino, et al., "Enhancing Breast Cancer Screening With Urinary Biomarkers and Random Forest Supervised Classification: Comprehensive Investigation," *Journal of Pharmacy Biomedicine Analytical* 244 (2024): 116113, https://doi.org/10.1016/j.jpba.2024.116113.

34. D. Stoessel, J. P. Stellmann, A. Willing, et al., "Metabolomic Profiles for Primary Progressive Multiple Sclerosis Stratification and Disease Course Monitoring," *Frontiers in Human Neuroscience* 12 (2018): 226, https://doi.org/10.3389/fnhum.2018.00226.

35. F. Rohart, B. Gautier, A. Singh, and K. A. Le Cao, "Mixomics: An R Package for 'Omics Feature Selection and Multiple Data Integration," *PLoS Computational Biology* 13, no. 11 (2017): e1005752, https://doi.org/10.1371/journal.pcbi.1005752.

36. M. P. Reichhardt, U. Holmskov, and S. Meri, "Salsa—A Dance on a Slippery Floor With Changing Partners," *Molecular Immunology* 89 (2017): 100–110, https://doi.org/10.1016/j.molimm.2017.05.029.

37. C. X. Zhang, "The Protective Role of DMBT1 in Cervical Squamous Cell Carcinoma," *Kaohsiung Journal of Medical Sciences* 35, no. 12 (2019): 739–749, https://doi.org/10.1002/kjm2.12117.

38. G. K. C. Lee, H. Kang, J. Beeler-Marfisi, W. Sears, B. N. Lillie, and D. Bienzle, "Effects of Equine SALSA on Neutrophil Phagocytosis and Macrophage Cytokine Production," *PLoS One* 17, no. 3 (2022): e0264911, https://doi.org/10.1371/journal.pone.0264911.

39. G. Pitari, F. Malergue, F. Martin, et al., "Pantetheinase Activity of Membrane-Bound Vanin-1: Lack of Free Cysteamine in Tissues of Vanin-1 Deficient Mice," *FEBS Letters* 483, no. 2–3 (2000): 149–154, https://doi.org/10.1016/s0014-5793(00)02110-4.

40. M. Daugherty, B. Polanuyer, M. Farrell, et al., "Complete Reconstitution of the Human Coenzyme A Biosynthetic Pathway via Comparative Genomics," *Journal of Biological Chemistry* 277, no. 24 (2002): 21431–21439, https://doi.org/10.1074/jbc.m201708200.

41. C. Berruyer, L. Pouyet, V. Millet, et al., "Vanin-1 Licenses Inflammatory Mediator Production by Gut Epithelial Cells and Controls Colitis by Antagonizing Peroxisome Proliferator-Activated Receptor γ Activity," *Journal of Experimental Medicine* 203, no. 13 (2006): 2817–2827, https://doi.org/10.1084/jem.20061640.

42. Y. O. Mosaad, M. A. Hussein, H. Ateyya, et al., "Vanin 1 Gene Role in Modulation of iNOS/MCP-1/tgf-B1 Signaling Pathway in Obese Diabetic Patients," *Journal of Inflammation Research* 15 (2022): 6745–6759, https://doi.org/10.2147/jir.s386506.

43. ŞD. Küçük, E. Gezer, M. Çalan, and A. Yüksel, "Relationship Between Serum Vanin 1 Level and Metabolic Parameters in Patients With Type 2 Diabetes Mellitus," *International Journal of Diabetes in Developing Countries* 43, no. 5 (2023): 801–806, https://doi.org/10.1007/s13410-022-01153-5.

44. A. Ostman, Q. Yang, and N. K. Tonks, "Expression of DEP-1, a Receptor-like Protein-Tyrosine-Phosphatase, Is Enhanced With Increasing Cell Density," *Proceedings of the National Academy of Sciences of the USA* 91, no. 21 (1994): 9680–9684, https://doi.org/10.1073/pnas.91.21.9680.

45. J. Krüger, S. Brachs, M. Trappiel, et al., "Enhanced Insulin Signaling in Density-Enhanced Phosphatase-1 (DEP-1) Knockout Mice," *Molecular Metabolism* 4, no. 4 (2015): 325–336, https://doi.org/10.1016/j.molmet.2015.02.001.

46. J. Ulke, S. Chopra, O. L. Kadiri, et al., "PTPRJ Is a Negative Regulator of Insulin Signaling in Neuronal Cells, Impacting Protein Biosynthesis, and Neurite Outgrowth," *Journal of Neuroendocrinology* 36, no. 12 (2024): e13446, https://doi.org/10.1111/jne.13446.

47. T. Shintani, S. Higashi, R. Suzuki, et al., "Ptprj Inhibits Leptin Signaling, and Induction of Ptprj in the Hypothalamus Is a Cause of the Development of Leptin Resistance," *Scientific Reports* 7, no. 1 (2017): 11627, https://doi.org/10.1038/s41598-017-12070-7.

48. E. Garcia, I. Shalaurova, S. P. Matyus, et al., "Ketone Bodies Are Mildly Elevated in Subjects With Type 2 Diabetes Mellitus and Are Inversely Associated With Insulin Resistance as Measured by the Lipoprotein Insulin Resistance Index," *Journal of Clinical Medicine* 9, no. 2 (2020): 321, https://doi.org/10.3390/jcm9020321.

49. Y. M. Han, T. Ramprasath, and M. H. Zou, "β-Hydroxybutyrate and Its Metabolic Effects on Age-Associated Pathology," *Experimental and Molecular Medicine* 52, no. 4 (2020): 548–555, https://doi.org/10.1038/s12276-020-0415-z.

50. N. J. Byrne, S. Soni, S. Takahara, et al., "Chronically Elevating Circulating Ketones Can Reduce Cardiac Inflammation and Blunt the Development of Heart Failure," *Circ Heart Fail* 13, no. 6 (2020): e006573, https://doi.org/10.1161/circheartfailure.119.006573.

51. F. M. Finucane, M. F. Rafey, M. Leahy, P. O'Shea, T. O'Brien, and M. O'Donnell, "Weight Loss Is Proportional to Increases in Fasting Serum Beta-Hydroxybutyrate Concentrations in Adults With Severe Obesity Undergoing a Meal Replacement Programme," *Hum Nutr Metab* 32 (2023): 200192, https://doi.org/10.1016/j.hnm.2023.200192.

52. Y. Zhang, Z. Li, X. Liu, et al., "3-hydroxybutyrate Ameliorates Insulin Resistance by Inhibiting Pparγ Ser273 Phosphorylation in Type 2 Diabetic Mice," *Signal Transduction and Targeted Therapy* 8, no. 1 (2023): 190, https://doi.org/10.1038/s41392-023-01415-6.

53. P. Borel, D. Preveraud, and C. Desmarchelier, "Bioavailability of Vitamin E in Humans: An Update," *Nutrition Reviews* 71, no. 6 (2013): 319–331, https://doi.org/10.1111/nure.12026.

54. Q. Jiang, "Natural Forms of Vitamin E: Metabolism, Antioxidant, and Anti-Inflammatory Activities and Their Role in Disease Prevention and Therapy," *Free Radical Biology and Medicine* 72 (2014): 76–90, https://doi.org/10.1016/j.freeradbiomed.2014.03.035.

55. S. Waniek, R. Di Giuseppe, S. Plachta-Danielzik, et al., "Association of Vitamin E Levels With Metabolic Syndrome, and MRI-Derived Body Fat Volumes and Liver Fat Content," *Nutrients* 9, no. 10 (2017): 1143, https://doi.org/10.3390/nu9101143.

56. R. Wan, Y. Su, M. Zhu, and Y. Huang, "The Association Between Blood Vitamin E and Blood Pressure in an Adult Population With and Without Diabetes Mellitus," *Frontiers in Endocrinology* 15 (2024): 1431293, https://doi.org/10.3389/fendo.2024.1431293.

57. T. Kim and J. Kang, "Association Between Serum Retinol and α-tocopherol Levels and Metabolic Syndrome in Korean General Population: Analysis of Population-Based Nationally Representative Data," *Nutrients* 12, no. 6 (2020): 1689, https://doi.org/10.3390/nu12061689.

58. C. B. Park, S. B. Lee, and D. D. Ryu, "L-Pyroglutamate Spontaneously Formed From L-Glutamate Inhibits Growth of the Hyperthermophilic Archaeon Sulfolobus Solfataricus," *Applied and Environmental Microbiology* 67, no. 8 (2001): 3650–3654, https://doi.org/10.1128/aem.67.8.3650-3654.2001.

59. W. Yan, S. Wu, Q. Liu, Q. Zheng, W. Gu, and X. Li, "The Link Between Obesity and Insulin Resistance Among Children: Effects of Key Metabolites," *Journal of Diabetes* 15, no. 12 (2023): 1020–1028, https://doi.org/10.1111/1753-0407.13460.

60. Y. Zhang, H. Zhao, B. Liu, et al., "Human Serum Metabolomic Analysis Reveals Progression for High Blood Pressure in Type 2 Diabetes Mellitus," *BMJ Open Diabetes Res Care* 9, no. 1 (2021): e002337, https://doi.org/10.1136/bmjdrc-2021-002337.

61. M. Tian, S. Ma, Y. You, et al., "Serum Metabolites as an Indicator of Developing Gestational Diabetes Mellitus Later in the Pregnancy: A Prospective Cohort of a Chinese Population," *Journal of Diabetes Research* 2021 (2021): 8885954, https://doi.org/10.1155/2021/8885954.

Supporting Information

Additional supporting information can be found online in the Supporting Information section.

Supporting Information S1: dmrr70090-sup-0001-suppl-data.docx. **Figure S1**: ROC curve derived from the top 15 metabolites proteins. **Figure S2**: ROC curve highlighting the top 15 metabolites. **Figure S3**: PLS-DA score plots of top 15 plasma proteins and metabolites. **Figure S4**: Pearson correlation analysis of the top 15 plasma proteins. **Figure S5**: Pearson correlation analysis between 15 plasma proteins, metabolites, BMI, and MetS presence. **Figure S6**: Pearson correlation analysis between the top 15 plasma metabolites. **Figure S7**: Plasma metabolite enrichment analysis. **Figure S8**: Plasma protein enrichment analysis. **Figure S9**: PLS-DA score plots of top 15 plasma proteins in the Case Control comparison. **Figure S10**: PLS-DA score plots of top 15 plasma proteins in the BMI comparison (normal weight, overweight and obese). **Figure S11**: PLS-DA score plots of top 15 plasma metabolites in the Case Control comparison. **Figure S12**: PLS-DA score plots of top 15 plasma metabolites in the BMI comparison (normal weight, overweight

and obese). **Figure S13**: Scatter plot of the first component across datasets. **Figure S14**: Clustered Image Map (CIM) of variables from multi-block sPLS-DA in component 1. **Table S1**: Demographic and clinical data of the 49 volunteers (mean ± sd). **Table S2**: Plasma proteins identified in the 4 study groups (n=49). **Table S3**: Plasma metabolites identified in the 4 study groups (n=49). **Table S4**: List of all proteins and metabolites names. **Table S5**: Main proteins/metabolites and clinical correlations. **Table S6**: Random Forest accuracy of plasma proteins and metabolites. **Table S7**: VIP socre accuracy of plasma proteins and metabolites. **Table S8**: Confusion matrix for proteins and metabolites based on data testing. **Table S9**: ROC curve accuracy of plasma proteins and metabolites. **Table S10**: Random Forest mean decrease accuracy of plasma proteins. **Table S11**: Random Forest mean decrease accuracy of plasma metabolites. **Table S12**: Significance analysis of proteome and metabolome microarrays. **Table S13**: Cross-validation of protein in protein and metabolite models. **Table S14**: Pair-wise PERMANOVA results. **Table S15**: Correlation table of the clinic data and plasma proteins. **Table S16**: Correlation table of the clinic and plasma metabolites. **Table S17**: Correlation table of plasma proteins and metabolites with BMI and MetS. **Table S18**: Enrichment analysis of plasma metabolites. **Table S19**: Enrichment analysis of plasma proteins. **Table S20**: Correlation table of the plasma proteins and metabolites.